Applied Physics A (2022) 128:661
https://doi.org/10.1007/s00339-022-05802-8

Applied Physics A
Materials Science & Processing

Kappa carrageenan/PEG-CuO nanoparticles as a multifunctional nanoplatform: digital colorimetric biosensor and anticancer drug nanocarrier

Aysun Karabatak[1] · Ferdane Danışman-Kalındemirtaş[2] · Ezgi Tan[1] · Serap Erdem-Kuruca[3] · Selcan Karakuş[1]

Received: 1 May 2022 / Accepted: 21 June 2022 / Published online: 11 July 2022

Abstract
The development of green multifunctional nanoformulation has been given great attention with unique anticancer activity and ultra-sensitive sensing properties in biomedical applications. This study investigated the smartphone-integrated colorimetric dopamine sensing platform and the anticancer activity of Kappa Carrageenan/PEG-CuO nanoparticles (κCA/PEG-CuO NPs). The characterization of the prepared κCA/PEG-CuO NPs was conducted using scanning electron microscopy (SEM), high-resolution transmission electron microscopy (HRTEM), X-ray diffraction analysis (XRD), zeta-potential, Fourier transform infrared spectroscopy (FTIR), and ultraviolet–visible (UV–Vis) techniques. The surface characterization revealed that the obtained NPs had a spherical surface in the particle-size range of 5–10 nm. With a high coefficient of correlation ($R^2 = 0.982$), the digital colorimetric κCA/PEG-CuO NPs-based biosensor detected dopamine in a wide concentration range of 0.1–100 μM and a low limit of detection (LOD) of 504 nM in 0.1 M phosphate buffer solution (PBS) (pH 7.4). In addition, the cytotoxicity of the prepared κCA/PEG-CuO NPs in living cells (HepG2 hepatocellular carcinoma), MIA PaCa-2 pancreatic cancer cells, and HUVEC (human umbilical vein endothelial cells) was investigated, which proved that κCA/PEG-CuO NPs exhibited high anticancer activity against MIA PaCa-2 pancreatic cancer cells. In conclusion, experimental results showed that multifunctional κCA/PEG-CuO NPs are both a promising biosensor for dopamine detection and an effective nanocarrier for pancreatic cancer therapy.

Keywords Cisplatin · Multifunctional nanoparticle · Pancreatic cancer · Dopamine biosensor

1 Introduction

Recent developments in the design of smart multifunctional NPs have heightened the need for sensors and drug delivery systems based on nanochemistry. These NPs have a unique surface, biological, and physicochemical properties for the fabrication of therapeutic nanoagents and sensitive electrodes in a small size range of 1–100 nm. Recent trends in the synthesis of metal/metal oxide NPs have led to new studies in biomedical applications [1, 2]. A number of researchers have reported to synthesizing multifunctional Au nanostars [3], Fe_3O_4/Ag nanocomposites [4], ZnO@CuS NPs [5], $TiO_2/ZnFe_2O_4$ nanospheres [6], and CuO NPs [7]. For this purpose, we designed κCA/PEG-CuO NPs that can be developed as both digital colorimetric sensing platforms and drug delivery systems. Smartphone supported personalized point-of-care (POC) diagnostics are fast becoming key devices in biomedical applications [8–11]. Nanostructure-based biosensors are commonly preferred as POC devices due to their portable, selective, sensitive, reliable, and rapid detection of target analytes using smartphone cameras in emerging technologies [12–14]. With this approach, scientific studies focus on portable, rapid, and high-performance digital colorimetric biosensors instead of high-cost traditional instruments such as chromatography and mass spectroscopy in sensor applications [15–18]. Furthermore, digital colorimetric biosensors are a new generation of mobile sensing platforms as a portable and easy-to-use device to detect

✉ Selcan Karakuş
selcan@iuc.edu.tr

1 Department of Chemistry, Faculty of Engineering, Istanbul University-Cerrahpasa, Avcılar, 34320 Istanbul, Turkey

2 Department of Physiology, Erzincan Faculty of Medicine, Erzincan Binali Yildirim University, 24100 Erzincan, Turkey

3 Department of Physiology, Istanbul Faculty of Medicine, Istanbul University, 34093 Istanbul, Turkey

biomolecules, store the experimental results in the cloud, and provide wireless access for future sensor applications. In digital colorimetric biosensing, the red, green, and blue (RGB) color values of the digital image are a major factor in sensor applications, and they play a key role in the detection of target biomolecules due to the particular color [0,0,0] for the black channel and [255,255,255] for the white color [19, 20]. The digital color image is commonly represented by a bit depth ranging from 8 to 24 with RGB components. The evaluation of RGB values of digital images has been reported as a sign of colorimetric response in a different pixel range from 8 to 24 bits in food and biomedical applications [21, 22].

Recently, digital colorimetric biosensors have become the most potent and commonly used sensor platforms for the monitoring of dopamine levels in media using the RGB method. In a previous study, Chellasamy et al. developed a novel smartphone-integrated colorimetric sensor for the detection of dopamine in plasma of old men and geriatric women using blue–green fluorescent carbon quantum dots with a limit of detection (LOD) values in the range of 6 to 8 nM [12]. In another study, Wang et al. fabricated selective boron and nitrogen co-doped silicon-carbon-dots-based colorimetric sensor for the detection of dopamine with an LOD of 1.58 ng mL^{-1}[23]. Razavi and co-workers reported that bismuth ferrite oxide nanoparticle-based sensors achieved high performance for the detection of dopamine with a linear range from 0.15 to 50 μM and a detection limit of 51 nM [24]. However, there are limited studies based on digital colorimetric nano-biosensors for the detection of dopamine to overcome drawbacks such as the high cost of preparation, difficult manufacturing process, low stability, biological inertness, and low biocompatibility. For this reason, we proposed an efficient and selective κCA/PEG-CuO NPs-based digital colorimetric sensing system for dopamine in this study. The κCA/PEG-CuO NPs-based digital colorimetric images were collected by a smartphone for the detection of dopamine, and these images were analyzed using a simple and low-cost RGB method for quantitatively analyzing dopamine concentrations. In this study, the cancer activity of nanostructures was also investigated.

As is known, cancer is one of the most important health problems in the world. While it is expected that there will be more than 25 million cancer cases each year until 2025, the incidence of cancer is expected to increase further in the coming decades [25, 26]. Although there are many treatment options such as surgery, radiotherapy, and chemotherapy in cancer treatment, survival rates are still low in patients after treatment. For these reasons, promising new strategies for cancer therapy continue to be investigated [27–29]. Therefore, nanostructure-based targeted drug delivery systems for cancer therapy have attracted increasing attention to enhance drug accumulation in cancer cells and therapeutic efficacy, and reduce side effects of drugs. Previous research has shown that nanoparticles with particle sizes ranging from 20 to 100 nm tend to accumulate and remain in tumor tissue. With this effect, called the enhanced permeability and retention (EPR) effect, nanoparticles pass into the interstitial space thanks to the increased permeability in the tumor vasculature, while suppressed lymphatic filtration allows them to stay there [30]. A considerable amount of literature has been published based on the penetration of multifunctional NPs for therapeutic applications [31]. These studies showed that the penetration of NPs into tumors could be easier due to their excellent morphology and surface properties such as size, surface charge, and shape [32]. In this study, we also investigated the cytotoxicity activity of cisplatin-loaded κCA/PEG-CuO NPs in living cells (HepG2 hepatocellular carcinoma), MIA PaCa-2 pancreatic cancer cells, and HUVEC (human umbilical vein endothelial cells). In conclusion, the experimental results showed that multifunctional κCA/PEG-CuO NPs as an anticancer drug delivery system and biosensor are a possibility for future applications in healthcare.

2 Experimental section

2.1 Chemicals

Polyethylene glycol 400 (PEG400) (molecular weight: 400 kDa) was obtained from Fluka (Switzerland). The cell lines were obtained from the American Type Culture Collection (ATCC, USA). MTT cell proliferation assay kit, Dulbecco's Modified Eagle's Medium (DMEM), dimethylsulfoxide (DMSO), fetal bovine serum (FBS) penicillin, streptomycin, trypsin, Copper (II) chloride anhydrous, (purity ≥ 99.99%), κCA (sulfated plant polysaccharide), glucose (D- (+)-Glucose monohydrate) (purity ≥ 99.0%), lactose (α-Lactose monohydrate) (purity ≥ 99%), fructose (D(−)Fructose) (purity ≥ 99%), maltose (D-(+)-Maltose monohydrate) (purity ≥ 99%), and urea (purity ≥ 99%) were provided from Sigma-Aldrich Company (Germany). Cisplatin was obtained from Koçak Pharma Company (Turkey). Ethanol (purity ≥ 99.5%), sodium hydroxide, ethyl alcohol (purity ≥ 99%), and isopropyl alcohol (purity ≥ 99.5%) were purchased from Merck Company (Germany). All samples were filtered using 0.45- and 0.22-micron retention of sterile syringe filters. All chemicals were analytical grade and used as received without further purification.

2.2 Preparation of multifunctional κCA/PEG-CuO NPs and drug-loaded κCA/PEG-CuO NPs

The multifunctional κCA/PEG-CuO NPs were prepared using a green ultrasonic method. 0.5 g of κCA was dissolved

in 250 mL of distilled water (agitation speed: 500 rpm), 0.25 mL of PEG400 was added to the κCA solution. 0.84 g of $CuCl_2$ was dissolved in 50 mL of distilled water at an agitation speed of 200 rpm. 0.1 g of NaOH was dissolved in 50 mL of distilled water at an agitation speed of 200 rpm. The 50 mL of $CuCl_2$ solution was added drop by drop into the κCA/PEG solution, and 2 mL of NaOH solution was added to the solution. Finally, the sample was sonicated for 30 min at an amplitude frequency of 30% and filtered using a 0.22-micron retention sterile syringe filter. To obtain cisplatin-loaded κCA/PEG-CuO NPs, 0.05 mg/mL cisplatin was added to the solution of κCA/PEG-CuO NPs, and it was vortexed at maximum speed for 3 min and kept for 1.5 h. It was kept in a black glass in the fridge at + 4 °C until use.

2.3 Characterization part

The chemical and surface properties of the prepared κCA/PEG-CuO NPs and drug-loaded κCA/PEG-CuO NPs were determined using various characterization techniques such as scanning electron microscopy (SEM) (JEOL JMS-7001F) with gold coating process at 20 kV of the accelerating voltage, high-resolution transmission electron microscopy (HRTEM) (HighTech HT7700) with a 100 kV of acceleration voltage, X-ray diffraction analysis (XRD) (Rigaku Miniflex 600) with Cu Kα radiation at 40 kV and 15 mA, and Fourier transform infrared spectroscopy (FTIR) (Perkin Elmer) in the frequency range from 400 to 4000 cm^{-1}. The prepared κCA/PEG-CuO NPs were examined using an ultraviolet–visible (UV–Vis) spectrophotometer (TG + 80 Model) at 207 nm wavelength. The zeta-potential results were performed on the Horiba SZ-100 nanoparticle analyzer at room temperature. A smartphone (Casper VIA F20, Turkey) was used for the determination of RGB values of via digital images using 48MP + 5MP + 2MP + 2MP smartphone cameras.

2.4 Cell culture studies

The cells were incubated in 5% CO_2 and 95% O_2 at 37 °C, and when the cells were confluent 70–80%, they were passaged. After, penicillin (100.000 U/L), streptomycin (100.000 g/L), and 10% FBS were added to the medium of the cell culture.

2.5 Evaluation of cell viability by MTT test

In the present study, HepG2 (hepatocellular carcinoma cells), MiaPaCa-2 (pancreatic cancer cells), and normal HUVEC cells (human umbilical vein endothelial cell lines) were procured from the ATCC (American Type Culture Collection, VA). Dulbecco's-Modified-Eagle-Medium (DMEM) added 10% FBS, streptomycin (100 μg/mL) and penicillin (100 units/mL,) were used to culture the cells at 37 °C, in 95% O_2 and 5% CO_2 atmosphere. Cancer and normal cells were passaged by trypsin when the cells reached certain confluency. MTT assay (3-(4,5-dimethylthiazol-2-yl)-2,5-diphenyltetrazolium bromide) was used to evaluate the cytotoxicity of the κCA/PEG-CuO NPs, Cis, and Cis-loaded κCA/PEG-CuO NPs [33]. For this, the κCA/PEG-CuO NPs were diluted to 1:2, 1:4, and 1:8 (v/v) ratios using DMEM to perform the MTT test. Then, Cis was loaded on κCA/PEG-CuO NPs with a Cis concentration of 0.5, 1, 2, 5, and 10 μg/mL. Accordingly, concentrations of κCA/PEG-CuO NPs changed as 1/20, 1/10, 1/5, 1/2, and 1, respectively, in the Cis-loaded κCA/PEG-CuO NPs. In addition, the cells were seeded, and the number of cells for each cell group was 10^5/mL and 90 μL in 96-well plates. Then, 10 μl of prepared sample concentration was added. The cells were incubated at 37 °C, in 95% O_2, and 5% CO_2 atmosphere for 72 h. After 72 h, 10 μL of MTT (5 mg/mL) solution was added to each well and incubated for 3 h. Then, 100 μL of DMSO was added and, after shaking the plate, it was read in an ELISA plate reader at 570 nm wavelength. All experiments were repeated at least three times.

2.6 Evaluation of digital colorimetric κCA/PEG-CuO NPs-based biosensor

For the analyte preparation process, the target analyte (dopamine) was prepared in different concentrations ranging from 0.1 to 100 μM for the colorimetric detection of dopamine in colorimetric smartphone measurements. All κCA/PEG-CuO NPs-based biosensor measurements were carried out against 10 μM of glucose, lactose, maltose, fructose, urea, isopropyl alcohol, ethyl alcohol, and dopamine using the RGB method. All images of the smartphone camera supported digital colorimetric κCA/PEG-CuO NPs-based biosensors were used to investigate the detection of dopamine in 0.1 M phosphate buffer solution (PBS) (pH = 7.4) medium. For the detection of the target analyte, 2 mL of κCA/PEG-CuO NPs were placed in a sterile centrifuge tube and the target analyte was dropped on the sample in a wide concentration range from 0.1 to 100 μM and kept for 1 min at 25 °C. All images of κCA/PEG-CuO NPs-based biosensors were taken using a Casper via F20 model smartphone camera with a resolution of 1600 × 1200 pixels using a screen size of 6.55 inches. Then, all images of κCA/PEG-CuO NPs-based biosensors were analyzed using a color histogram software (ImageJ 1.51q) corresponding to the differences of RGB values.

The euclidean distance (ΔE) (Eq. 1) and response (%) (S) (Eq. 2) values of κCA/PEG-CuO NPs-based biosensors were calculated for the quantitative colorimetric detection of the target analyte using RGB data in the range from [0,0,0] black channel and [255,255,255] white color [34, 35]. The limit of

detection (LOD) of the biosensor was calculated using the slope of the plot of Log(C)-S (%) (Eq. 3 and Eq. 4)

$$\Delta E = \sqrt{(R_i - R_0)^2 + (G_i - G_0)^2 + (B_i - B_0)^2}, \quad (1)$$

where R_i denotes the red color value of the sample, R_o the red color value of the reference, G_i the green color value of the sample, G_O the green color value of the reference, B_i the blue color value of the sample, and B_o the blue color value of the reference

$$S = 100\frac{x_c - x_0}{x_0 - x_{ref}}\ [\%] \quad (2)$$

$$S(\%) = mLog(C) + n \quad (3)$$

$$LOD = 3.3x\sigma/m, \quad (4)$$

where S (%): response (%), c: concentration, x_c: sensor signal value, x_0: blank signal value, σ: the standard deviation of the regression line, m: slope, and x_{ref}: reference signal value [36].

3 Results and discussion

3.1 Characterizations

The surface and chemical properties of multifunctional κCA/PEG-CuO NPs and Cis-loaded κCA/PEG-CuO NPs were investigated by employing SEM, HRTEM, FTIR, zeta potential, and XRD techniques. In Fig. 1, SEM images of (a) κCA/PEG-CuO NPs, HRTEM images of (b) κCA/PEG-CuO NPs, (c) Cis-loaded κCA/PEG-CuO NPs (×200 magnification), (d) Cis-loaded κCA/PEG-CuO NPs (×300 magnification), and (e) particle-size distributions of Cis-loaded κCA/PEG-CuO NPs were presented. To investigate the morphology of CuO NPs in the polymer blend matrix, the SEM image of the κCA/PEG-CuO NPs was evaluated. The SEM micrograph of κCA/PEG-CuO NPs revealed the heterogeneous structure of the nanostructure with spherical particles depending on the CuO particles (Fig. 1a).

The HRTEM technique was carried out to understand the surface characteristics of the κCA/PEG-CuO NPs and Cis-loaded κCA/PEG-CuO NPs with different magnifications such as ×200 and ×300 (Fig. 1.b-e). According to the HRTEM images, the particle-size distributions of nanostructures ($n = 50$) were determined using a simple ImageJ software. The κCA/PEG-CuO NPs were observed to be spherical in shape, and the particle size of the prepared κCA/PEG-CuO NPs was found to be ~6 nm. Furthermore, HRTEM images of the prepared Cis-loaded κCA/PEG-CuO NPs revealed that the drug-loaded nanocarrier had spherical particles in particle sizes ranging from 7 to 10 nm. Distribution of the primary particle size in κCA/PEG-CuO NPs agglomerates. It was clear that the mean size was 6.77 nm with a standard deviation of 1.48 nm from TEM images. Consequently, we assumed that it occurred due to the presence of CuO NPs on the surface of nanocarriers which electrostatically interact with cisplatin leading to control of particle morphology and size. In a previous study, Cheni et al. developed a novel CuO NPs@Starch based chemotherapeutic drug for the treatment of different cancers such as gastric, pancreatic, and colon cancers, and they observed similar spherical morphology of the nanostructure to our results [37].

To determine the functional groups and crystalline nature of nanostructures, FTIR spectra of (a) κCA/PEG, (b) κCA/PEG-CuO NPs, (c) cisplatin-loaded κCA/PEG-CuO NPs, and (d) XRD graph of κCA/PEG-CuO NPs are given in Fig. 2a-c. According to the FTIR graph of κCA-PEG (Fig. 2a), it was observed at 3374.04 cm^{-1} (OH stretching), 2894.78 cm^{-1} (CH symmetric stretching band), 1638.52 cm^{-1} (OH stretching), 1451.90 cm^{-1}(C–H bending), 1352.41 cm^{-1} (C–H bending), 1246.39 cm^{-1} (sulfate stretching band), 1059.77 cm^{-1} (C–O-stretching vibrations), 923.25 cm^{-1} (C–H bending), and 824.65 cm^{-1} (C–H bending) [38]. In Fig. 2b, from the FTIR result of κCA/PEG-CuO NPs, it was found that the characteristic bands at 3368.24 cm^{-1} and 2892.65 cm^{-1} were due to the OH stretching and CH symmetric stretching bands, respectively. The peaks at 1643.60 cm^{-1}, 1527.42 cm^{-1}, 1376.38 cm^{-1}, 1239.86 cm^{-1}, 1065.60 cm^{-1}, 929.06 cm^{-1}, and 841.92 cm^{-1} were attributed to the OH stretching, asymmetric stretching vibrations of the carbonate ion, C–H bending, sulfate stretching band, C–O-stretching vibrations, C–C-stretching vibrations, and CH_2 rocking mode, respectively [39]. In the FTIR graph of κCA/PEG-CuO NPs, the weak peaks at 702.88 cm^{-1} and 523.32 cm^{-1} were attributed to the CuO-stretching vibration, respectively [40]. In Fig. 2c, the characteristic bands at 2870.82.65 cm^{-1}, 1750.35 cm^{-1}, 1457.71 cm^{-1}, 1358.22 cm^{-1}, 1183.94 cm^{-1}, 1083.73 cm^{-1}, 928.34 cm^{-1}, 872.42 cm^{-1}, and 754. 78 cm^{-1} were due to the CH symmetric stretching band, C = O stretching, CH_3 surface bending vibration, C–H bending, C = O-stretching vibration, C–O-stretching vibrations, C–C-stretching vibrations, CH_2 rocking mode, and the CuO-stretching vibration, respectively. Moreover, the disappearance of the characteristic peaks at 3368.24 cm^{-1}, 1643.60 cm^{-1}, and 1239.86 cm^{-1} corresponding to the OH group and sulfate stretching band was observed, which could be related to the electrostatic interaction between the anionic sulfonate groups of PEGlayted κCA and cationic platin drug in the presence of CuO NPs. According to the XRD results, we observed that the prepared κCA/PEG-CuO NPs showed

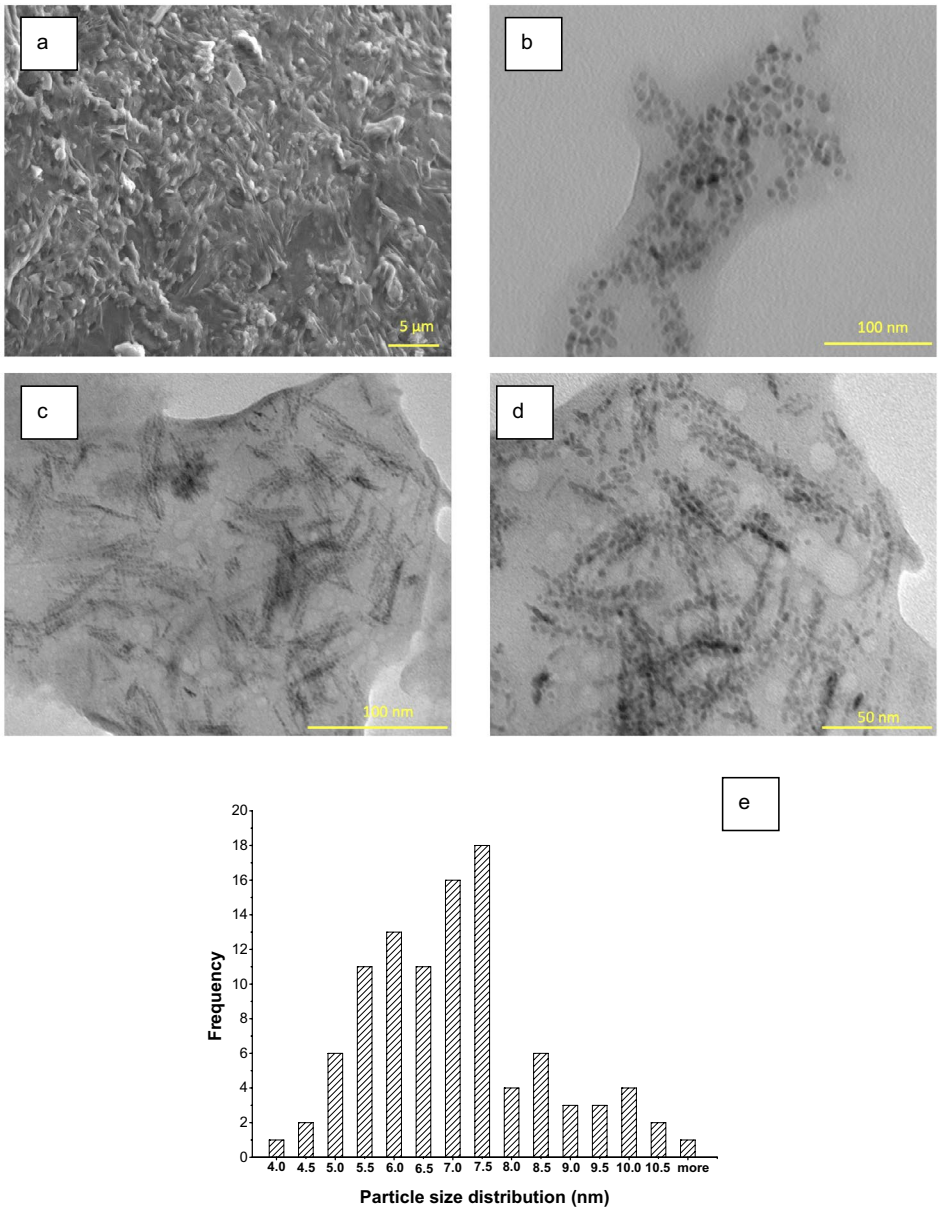

Fig. 1 SEM image of **a** κCA/PEG-CuO NPs, HRTEM images of **b** κCA/PEG-CuO NPs, **c** cisplatin-loaded κCA/PEG-CuO NPs (x200k), **d** cisplatin-loaded κCA/PEG-CuO NPs(x300k), and **e** particle-size distribution of κCA/PEG-CuO NPs

no sharp XRD peaks. However, a small scattering was found at 2θ = 31.9° corresponding to (110) planes of the monoclinic CuO [41] and confirmed the amorphous nature of κCA/PEG-CuO NPs (Fig. 2d). In Fig. 2e, the zeta-potential analysis graph of prepared κCA/PEG-CuO NPs was presented. The zeta-potential values of the prepared κCA/PEG-CuO NPs ranged from − 35 mV to + 10 mV, and were found to be at − 0.18 mV due to the electrostatic repulsive forces of nanoparticles and a small degree of agglomeration. The negative value for the zeta potential of the prepared κCA/PEG-CuO NPs enabled colloidal stability for the hydrophobic CuO NPs [42].

3.2 Detection of dopamine by the digital colorimetric κCA/PEG-CUO NPs-based biosensor

In this study, the digital colorimetric detection of dopamine was investigated, and the experimental results were analyzed using naked eye observation and smartphone techniques. All images of samples were subsequently quantified using the RGB method.

In Fig. 3, all images of κCA/PEG-CuO NPs-based biosensors (a) in a concentration range of 0.1–100 µM of dopamine at pH = 7.4, (b) in the presence of 10 µM of different analytes, (c) the graph of Log C–ΔE, (d) the graph of Log C–S

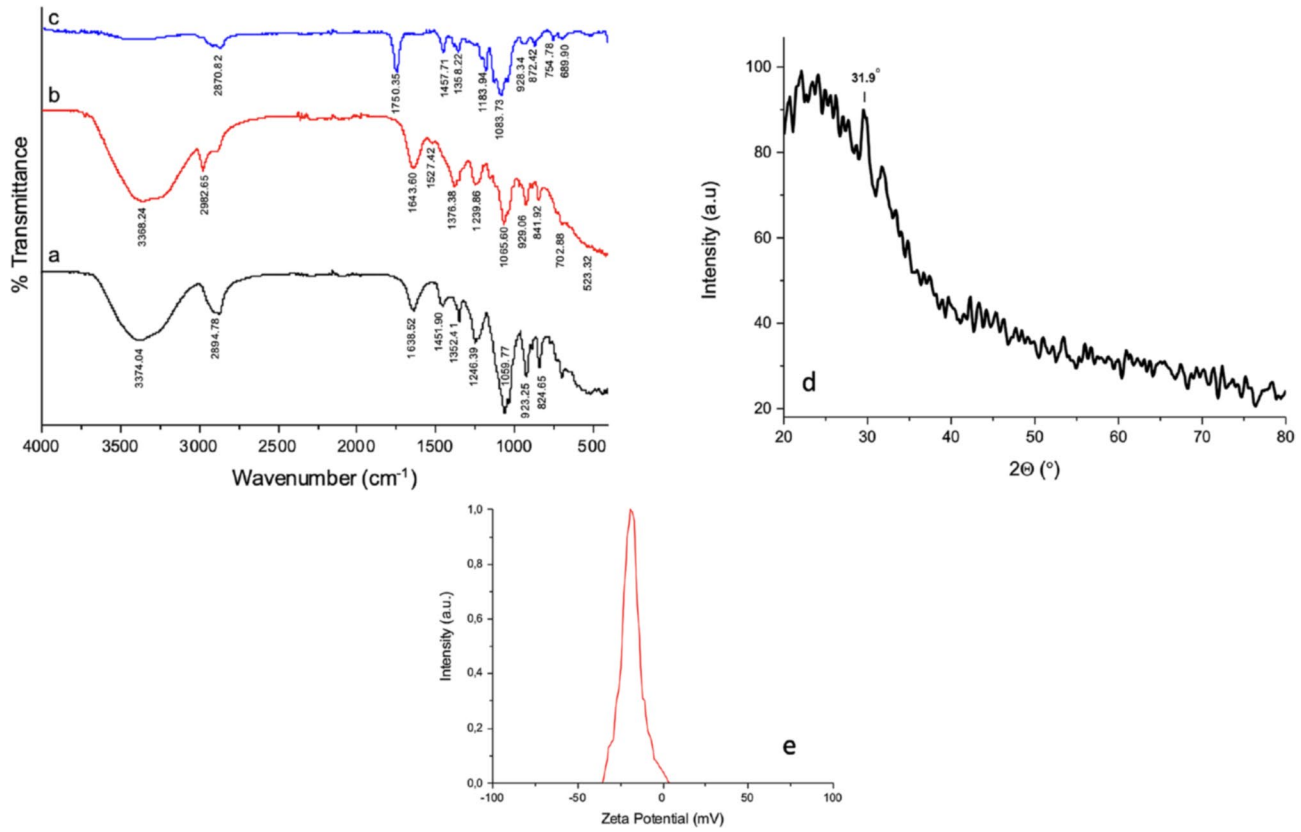

Fig. 2 FTIR spectra of **a** κCA/PEG, **b** κCA/PEG-CuO NPs, **c** cisplatin-loaded κCA/PEG-CuO NPs, **d** XRD graph of κCA/PEG-CuO NPs, and **e** zeta-potential analysis graph of synthesized κCA/PEG-CuO NPs

(%), (e) the selectivity of biosensors (a: glucose, b:lactose, c:maltose, d:fructose, e:urea, f:isopropyl alcohol, g:ethyl alcohol, and h:dopamine), UV–Vis absorption spectrum of (f) κCA/PEG, and (g) κCA/PEG-CuO NPs were given. RGB values of the prepared κCA/PEG-CuO NPs-based biosensors were calculated using the Image J software. The colorimetric κCA/PEG-CuO NPs-based dopamine biosensor selectively detected dopamine in the image with a color change from blue to black using the naked eye observing method. When dopamine in a concentration range of 0.1–100 μM was added to the κCA/PEG-CuO NPs solution, the blue color κCA/PEG-CuO NPs changed to black in 5 min (Fig. 3a). Moreover, images of κCA/PEG-CuO NPs-based biosensors in different analytes were used, and the visible color change was not observed by these biosensors in the presence of different analytes such as glucose, lactose, maltose, fructose, urea, isopropyl alcohol, and ethyl alcohol (Fig. 3b). According to the RGB imaging analysis of target analytes, values of ΔE of the κCA/PEG-CuO NPs-based biosensor were found to be 3.31, 5.61, 4.06, 11.92, 6.11, 18.59, 35.62, and 266.87 for glucose, lactose, maltose, fructose, urea, isopropyl alcohol, and ethyl alcohol, respectively (Fig. 3c). However, the value of ΔE of the κCA/PEG-CuO NPs-based biosensor was drastically changed in the increase from 35 to 267 with a wide concentration range of 0.1–100 μM (Fig. 3d). The experimental results of the digital colorimetric κCA/PEG-CuO NPs-based biosensor revealed that the proposed biosensor had a highly selective (Fig. 3e) and sensitive colorimetric dopamine detection performance with an LOD of 504.2 nm and a correlation coefficient value (R^2) of 0.9824 in a wide concentration range of 0.1–100 μM. We assumed that the colorimetric sensing mechanism was based on the interaction between the negative surface of CuO and the positively charged dopamine. It was a sign of the increase of contact time from 0 to 5 min. The RGB values changed, which could be related to the reduction of Cu^{2+} to Cu. Furthermore, we assumed that the digital colorimetric κCA/PEG-CuO NPs-based biosensor had a high sensitivity for dopamine with the oxidation reaction of dopamine, resulting in the formation of dopamine-o quinone by the two-electron two-proton ($2e^-$, $2H^+$) redox mechanism of dopamine [43]. In addition, the optical properties of the prepared κCA/PEG- and κCA/PEG-CuO NPs were determined using an ultraviolet–visible (UV–Vis) absorption spectrophotometer. According to the UV–Vis results, we observed that there was a maximum absorbance at 263 nm related to the CuO NPs and direct optical bandgap was found to be 4.7 eV [44] (Fig. 3f-g).

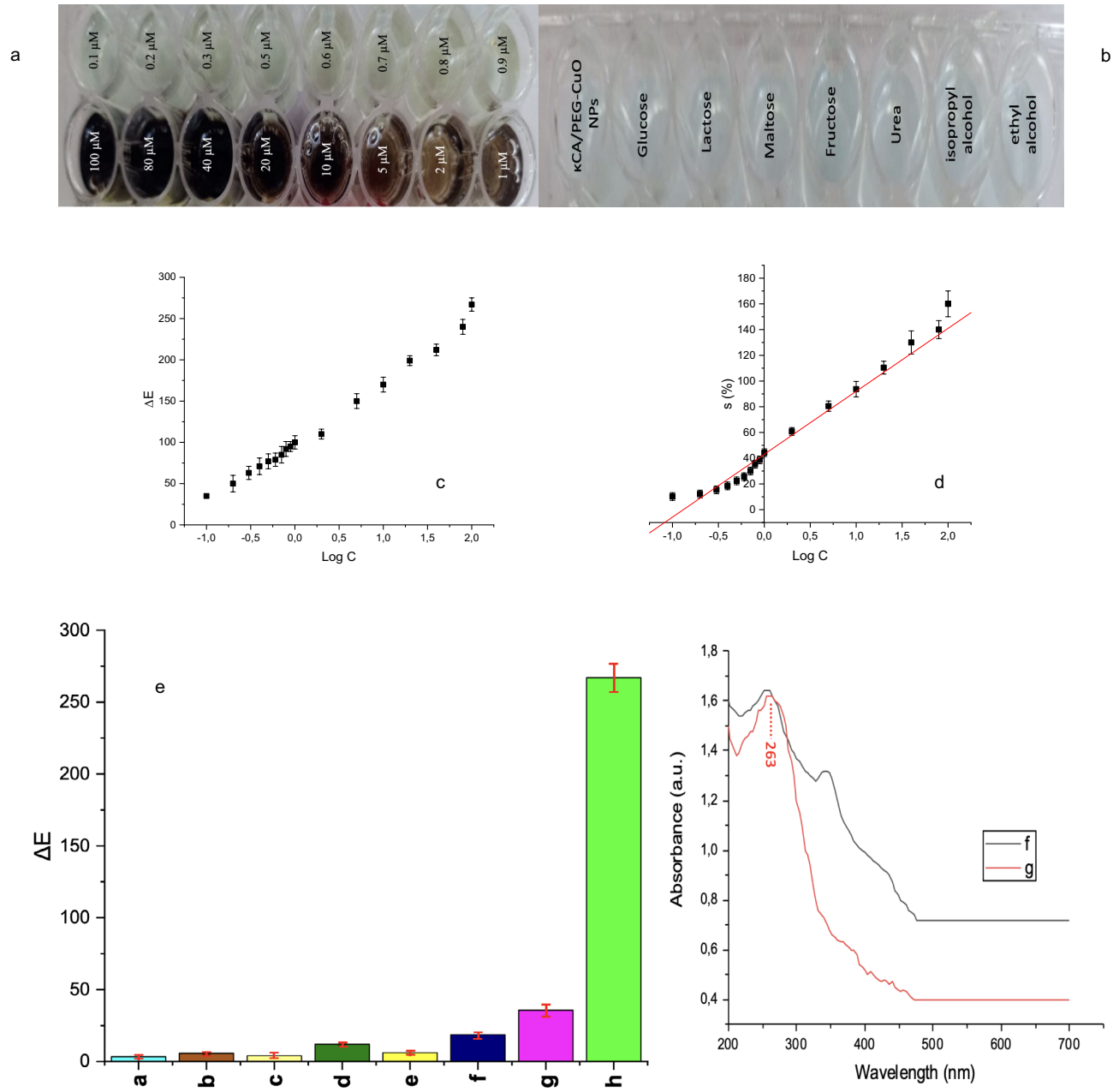

Fig. 3 All images of κCA/PEG-CuO NPs-based biosensors **a** in a concentration range of 0.1–100 µM of dopamine at pH = 7.4, **b** in the presence of 10 µM of different analytes, **c** the graph of Log C– ΔE, **d** the graph of Log C– S (%), **e** the selectivity of biosensors (a: glucose, b:lactose, c:maltose, d:fructose, e:urea, f:isopropyl alcohol, g:ethyl alcohol, and h:dopamine), UV–Vis absorption spectrum of **f** κCA/PEG, and **g** κCA/PEG-CuO NPs

In previous studies, many biosensors were focused on colorimetric measurements of different electrodes, such as ionic liquid tuned titanium dioxide nanostructures [45], multilayer Ti3C2 MXene, graphitized multi-walled carbon nanotubes and ZnO nanospheres [46], carbon quantum dots/copper oxide nanocomposite [47], core–shell polyparaphenylenediamine/titanium dioxide/multi-walled carbon nanotube nanocomposite [48], hollow zeolitic imidazolate framework [49], and CuO nanoparticle [50], ionic liquid functionalized drug-mediated silver nanostructures [51], and bismuth ferrite oxide NPs [24] for the detection of dopamine (Table 1). This study provided an exciting opportunity to advance our knowledge of digital selective and sensitive colorimetric κCA/PEG-CuO NPs-based dopamine biosensors using portable and simple smartphone algorithms for biomedical applications. Consequently, with colorimetric

Table 1 The comparison of colorimetric/electrochemical performance of the various electrodes for the dopamine detection

Electrodes	Experimental results	Ref
Ionic liquid tuned titanium dioxide nanostructures	LOD: 2.55×10^{-7} M and 7.67×10^{-8} M	[45]
Multilayer Ti3C2 MXene, graphitized multi-walled carbon nanotubes and ZnO nanospheres	LOD: 3.3 nM	[46]
Carbon quantum dots/copper oxide nanocomposite	LOD: 25.40 μM	[47]
Core–shell polyparaphenylenediamine/titanium dioxide/multi-walled carbon nanotube nanocomposite	LOD: 9.45×10^{-12} M	[48]
Hollow zeolitic imidazolate framework	LOD: 0.012 μM	[49]
CuO nanoparticle	LOD: 5.5×10^{-8} M	[50]
κCA/PEG-CuO NPs	LOD: 504 nM	This study

experimental results, the proposed biosensor is a promising green, low-cost and effective κCA/PEG-CuO NPs biosensor for monitoring of dopamine due to the occurrence of the redox mechanism (from Cu^{2+} to Cu).

3.3 Cytotoxic effects of κCA/PEG-CuO NPs

In this study, the cytotoxic activity of κCA/PEG-CuO NPs and Cis-loaded κCA/PEG-CuO NPs was determined using the MTT colorimetric test. HepG2 hepatocellular cancer cells and MIA Paca-2 pancreatic cancer cells were used.

The mechanism underlying cytotoxicity of nanoparticles may differ. Due to their small size, nanoparticles can more easily enter many tissues in the body. Size, shape, surface charge, and modifications play an important role in the cytotoxicity of nanoparticles. It is thought that NPs cause oxidative stress, especially with the production of reactive oxygen species, and as a result, cell functions are disrupted and cell death is caused [52]. ROS production may be one of the cytotoxicity mechanisms of nanoparticles, which can cause inflammation, oxidative stress, and as a result, damage to the cell membrane, proteins, and DNA [53]. Additionally, it has been reported that nanoparticles induce apoptosis by mediating various cellular pathways [54].

Figure 4 shows that κCA/PEG-CuO NPs alone are highly cytotoxic to HepG2 cancer cells. It is clearly seen that cytotoxicity of undiluted κCA/PEG-CuO NPs was 77% on HepG2 cells. Furthermore, it caused cell death at a rate of 58% with a 1:2 dilution rate. The IC_{50} value of κCA/PEG-CuO NPs, the concentration that inhibited half of HepG2

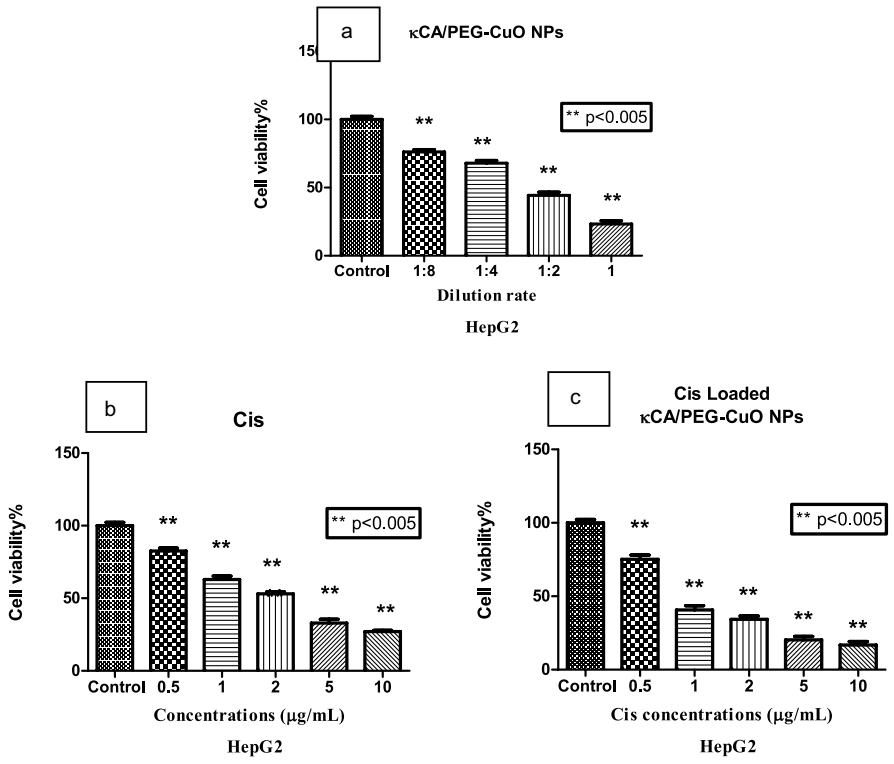

Fig. 4 The cytotoxic effects of κCA/PEG-CuO NPs (**a**), Cisplatin (**b**), and cisplatin-loaded κCA/PEG-CuO NPs (**c**) on HepG2 cancer cells. To investigate the toxicity of κCA/PEG-CuO NPs (a) and Cis-loaded κCA/PEG-CuO NPs were prepared as 1/20, 1/10, 1/5, 1/2, and 1 dilution ratio, respectively. The same Cis concentration was used in the compounds in graphs (b) and (c). Statistical significance is shown with $^{**}p<0.05$ compared to the control group. All tests were repeated three times. The samples were evaluated with Student's *t* test analysis and differences were considered significant at $p<0.05$. GraphPad software was used

cells, was nearly a 1:3 dilution ratio. That is, κCA/PEG-CuO NPs had strong cytotoxicity in hepatocellular cancer cells even when diluted nearly threefold. Considering the pancreatic cancer MIA PaCa-2 cells, which are known to be highly aggressive, it was cytotoxic on 42% of the cells with undiluted κCA/PEG-CuO NPs (Fig. 3). More importantly, when we evaluated non-cancer HUVEC cells, undiluted κCA/PEG-CuO NPs showed only a 28% cytotoxic effect on normal HUVEC. In this case, the κCA/PEG-CuO NPs demonstrated specific cytotoxicity against HepG2 and MIA PaCa-2 cancer cells (Fig. 4, 5, 6). In addition, the IC_{50} of free Cis was 2.9 µg/ml in HepG2 cells, while the IC_{50} value of Cis-loaded κCA/PEG-CuO NPs was 0.9 µg/ml, despite containing less Cis. Regarding MIA PaCa-2 cells, the IC_{50} of Cis was found to be 12.8, while the IC_{50} of Cis-loaded κCA/PEG-CuO NPs was found to be 3.5. In HUVEC cells, κCA/PEG-CuO NPs had an IC_{50} value of 4.8 µg/ml. As a result, κCA/PEG-CuO NPs significantly increased the effect of Cis 3.22-fold with Cis-loaded κCA/PEG-CuO NPs on HepG2 cells and 3.65-fold on MiaPaCa cells (Table 2, Fig. 3, 4, 5, 6). As known, nanocarriers increase the biocompatibility and therapeutic effect of anticancer drugs. In the literature, it was reported that there was a significant decrease in side effects. With these advantages, CuO NPs are to solve problems related to dose-dependent [55–57]. For this reason, the synthesized κCA/PEG-CuO was used as an anticancer nanoagent for the Cis delivery system. Therefore, the drug can more effectively be accumulated in cancer cells and nanocarriers can improve the bioavailability and therapeutic effect of anticancer drugs [58]. Accordingly, Cis-loaded κCA/PEG-CuO is expected to have a lower IC_{50} than Cis. As a result, the κCA/PEG-CuO NPs were most cytotoxic in HepG2 cells, while it had low cytotoxicity in HUVEC cells. In addition, it was observed that when cisplatin was loaded to κCA/PEG-CuO NPs, it increased the effect of cisplatin exponentially in both cancer cell groups. In the light of these findings, it seems possible to reduce the side effects of cisplatin using κCA/PEG-CuO nanocarrier and lower doses of cisplatin.

In Fig. 7, HepG2 cells in the control group have cell density and the cells form large groups in connection with each other. Morphological changes are remarkable in all treated κCA/PEG-CuO NPs, Cis, and Cis-loaded κCA/PEG-CuO NPs groups. In particular, it is seen that the intercellular connections have decreased, the number and density of cells have decreased by about half, and the cell groups have become smaller. MIA PaCa-2 cells have denser, more numerous spindle-shaped cells than in the control group.

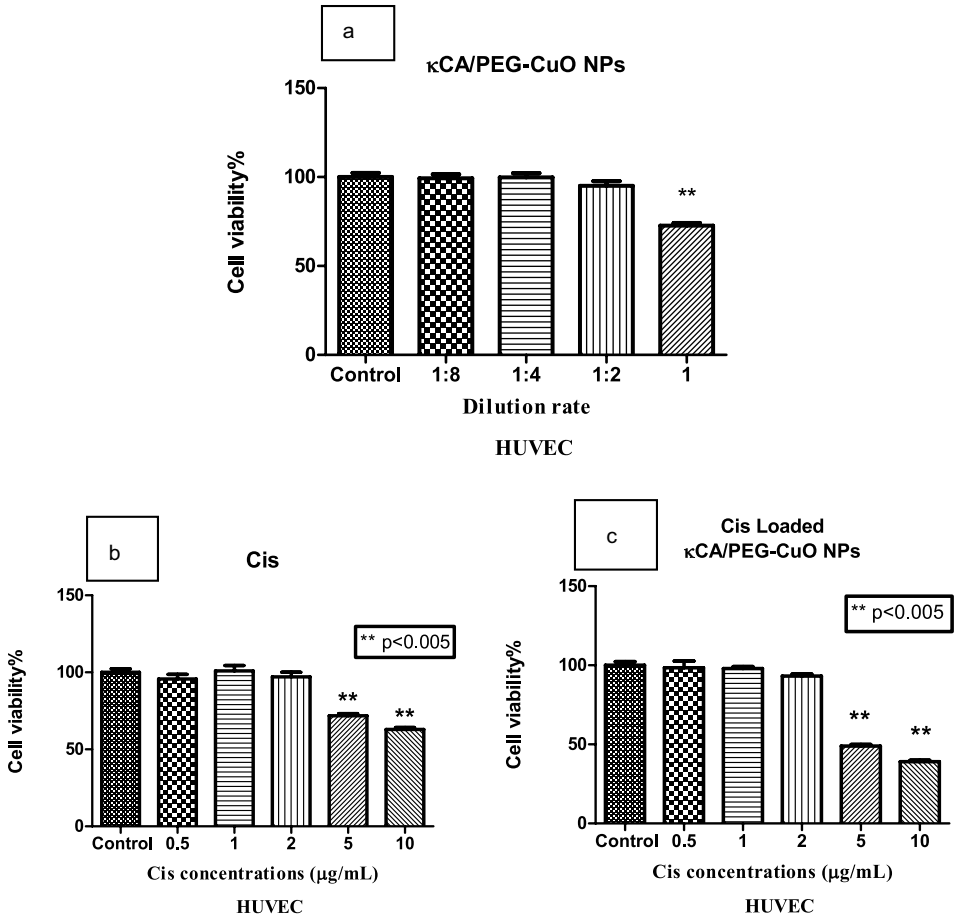

Fig. 5 The cytotoxic effects of κCA/PEG-CuO NPs (**a**), Cisplatin (**b**), and cisplatin-loaded κCA/PEG-CuO NPs (**c**) on normal HUVEC cells. To investigate the toxicity of κCA/PEG-CuO NPs (A) and Cis-loaded κCA/PEG-CuO NPs were prepared as 1/20, 1/10, 1/5, 1/2, and 1 dilution ratio, respectively. The same Cis concentration was used in the compounds in graphs (b) and (c). Statistical significance is shown with $^{**}p < 0.05$ compared to the control group. All tests were repeated 3 times. The samples were evaluated with student t-test analysis and differences were considered significant at $p < 0.05$. GraphPad software was used

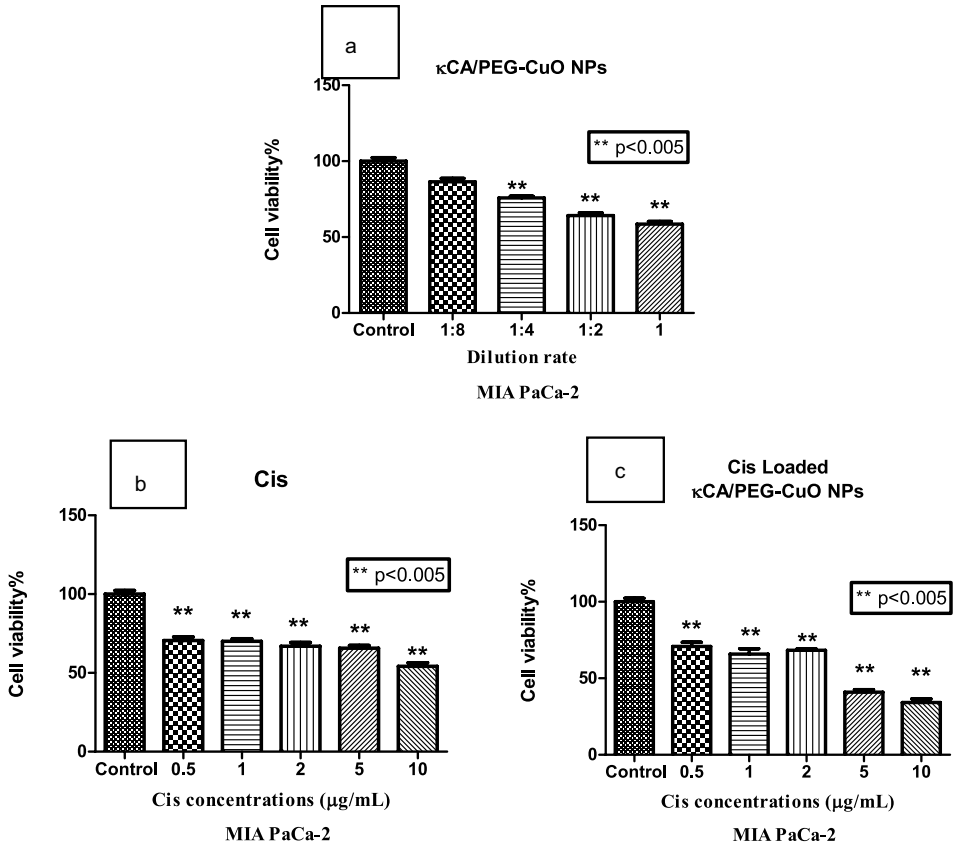

Fig. 6 The cytotoxic effects of κCA/PEG-CuO NPs (**a**), Cisplatin (**b**), and Cisplatin loaded κCA/PEG-CuO NPs (**c**) on MIA Paca-2 cancer cells. To investigate the toxicity of κCA/PEG-CuO NPs (a) and Cis Loaded κCA/PEG-CuO NPs were prepared as 1/20, 1/10, 1/5, 1/2, and 1 dilution ratio, respectively. The same Cis concentration was used in the compounds in graphs (b) and (c). Statistical significance is shown with $^{**}p < 0.05$ compared to the control group. All tests were repeated three times. The samples were evaluated with student t-test analysis and differences were considered significant at $p < 0.05$. GraphPad software was used

It is noteworthy that in the treated groups, the intercellular connections were lost, the cells shrank, and their numbers decreased significantly. In Fig. 7, it is seen that the morphological changes are consistent with the cytotoxic findings. In addition, the effects of Cis-loaded κCA/PEG-CuO NPs on in vitro drug profiles were studied at tumor pH 5.5. We assumed that the novel CuO NPs as smart pH-responsive drug nanocarriers could have a role in the in vivo release profiles of the anticancer drug Cis at different mediums such as gastrointestinal pH (1.2 and 7.4) and tumor pH (5.5) mediums in oral chemotherapies.

Table 2 IC_{50} values of κCA/PEG-CuO NPs, and Cis-loaded κCA/PEG-CuO NPs on HepG2, MiaPaCa, and HUVEC cells

IC_{50}* values		
	Cis (μg/mL)	Cis-loaded κCA/PEG-CuO NPs (μg/mL)
HepG2	2.9	0.9
MiaPaCa	12.8	3.5
HUVEC	> 10	4.8

Proliferation was evaluated by MTT, and IC_{50} values were taken after 72 h.

*IC_{50}: Concentration that inhibited cell growth by 50%

4 Conclusion

In this study, the novel κCA/PEG-CuO NPs was synthesized using a simple and cost-effective ultrasonic-assisted method at a room temperature of 25 °C. The green digital selective and sensitive κCA/PEG-CuO NPs-based dopamine biosensor was fabricated for their colorimetric dopamine detection and anticancer drug delivery systems. The proposed biosensor was investigated as an effective sensor for the detection of dopamine in biomedical applications. The digital colorimetric results showed that the dopamine biosensor had emerging high-performance characteristics, such as selectivity, sensitivity, and rapid detection. According to in vitro cytotoxicity results, it was observed that Cis-loaded κCA/PEG-CuO NPs had lower IC_{50} values than free Cis and showed selective cytotoxicity against cancer cells compared to control cells (HUVEC). These experimental findings confirm the multifunctional function of κCA/PEG-CuO NPs as drug carriers and sensors, demonstrating that they can be used in biomedical applications.

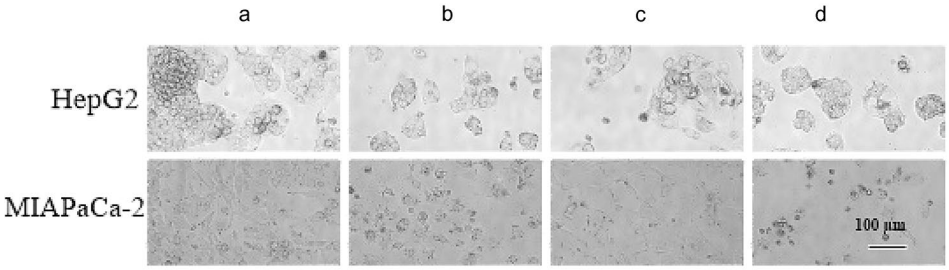

Fig. 7 **a** Light microscope (Magnification: X100) κCA/PEG-CuO NPs was used with 1:3 dilution rate on HepG2 cells and without dilution MIA PaCa-2 cells. Cis and Cis-loaded κCA/PEG-CuO NPs were used in IC_{50} values on HepG2 and MIA PaCa-2 cells. Morphological change of HepG2, MiaPaCa-2 cancer cells treated with κCA/PEG-CuO NPs (**b**), Cis (**c**), Cis-loaded κCA/PEG-CuO NPs, and **d** untreated.

Acknowledgements This work was supported by Scientific Research Projects Coordination Unit of Istanbul University-Cerrahpasa under Project Number: 36118.

Declarations

Conflicts of interest We declare that we have no conflict of interest.

References

1. F. Khosravi-Nejad, M. Teimouri, S. Jafari Marandi, M. Shariati, The highly sensitive impedimetric biosensor in label free approach for hepatitis B virus DNA detection based on tellurium doped ZnO nanowires. Appl Phy A: Mater Sci Process. (2019). https://doi.org/10.1007/s00339-019-2890-4
2. B. Cai, W. Mao, Z. Ye, J. Huang, Appl. Phys. A Mater. Sci. Process. **122**, 1 (2016)
3. S. Wang, Y. Zhang, Y. Li, K. Chen, Y. Dai, D. Zhou, A. Ali, S. Yang, X. Xu, T. Jiang, L. Zhu, Mater. Des. **205**, 109707 (2021)
4. T. Chen, S. Zhou, Z. Hu, X. Fu, Z. Liu, B. Su, H. Wan, X. Du, Z. Gao, Colloids Surf., A **626**, 127041 (2021)
5. H. Deng, Y. Yang, T. Zuo, T. Fang, Y. Xu, J. Yang, J. Zhang, Q. Shen, Nanomedicine: Nanotechnology. Biol Med **34**, 102399 (2021)
6. P. Suppuraj, G. Thirunarayanan, S. Rajalakshmi, V. Usha, N. Sundaramurthy, M. Swaminathan, I. Muthuvel, Mater Today: Procee **43**, 2134 (2021)
7. Z. Nakhaeepour, M. Mashreghi, M.M. Matin, A. NakhaeiPour, M.R. Housaindokht, Life Sci. **234**, 116758 (2019)
8. B. Purohit, A. Kumar, K. Mahato, P. Chandra, Curr Opin Biomed Eng **13**, 42 (2020)
9. G. Zhao, M. Li, Appl. Phys. A Mater. Sci. Process. **124**, 1 (2018)
10. M. Shariati, Appl. Phys. A Mater. Sci. Process. **123**, 1 (2017)
11. G. Biasotto, J.P.C. Costa, P.I. Costa, M.A. Zaghete, Appl. Phys. A Mater. Sci. Process. **125**, 1 (2019)
12. G. Chellasamy, S.R. Ankireddy, K.-N. Lee, S. Govindaraju, K. Yun, Mater Today Bio **12**, 100168 (2021)
13. K. Ponlakhet, K. Phooplub, N. Phongsanam, T. Phongsraphang, S. Phetduang, C. Surawanitkun, C. Buranachai, W. Loilome, W. Ngeontae, Food Chem. **384**, 132478 (2022)
14. A. Lopreside, L. Montali, B. Wang, A. Tassoni, M. Ferri, M.M. Calabretta, E. Michelini, Biosens. Bioelectron. **194**, 113569 (2021)
15. K. Salimiyan rizi, The smartphone biosensors for point-of-care detection of human infectious diseases: Overview and perspectives—A systematic review. Curr Opin Electrochem **32**, 100925 (2022)
16. P.B. Lillehoj, M.C. Huang, N. Truong, C.M. Ho, Lab Chip **13**, 2950 (2013)
17. H. Kim, Y. Jung, I.J. Doh, R.A. Lozano-Mahecha, B. Applegate, E. Bae, Smartphone-based low light detection for bioluminescence application. Sci Rep (2017). https://doi.org/10.1038/srep40203
18. S. Karakuş, G. Baytemir, N. Taşaltın, Appl Phy A **128**, 5 (2022)
19. G. de Carvalho Oliveira, C.C.S. Machado, D.K. Inácio, J.F. daSilveira Petruci, S.G. Silva, RGB color sensor for colorimetric determinations: evaluation and quantitative analysis of colored liquid samples. Talanta **241**, 123244 (2022)
20. T. Anazawa, M. Yamazaki, S. Yamamoto, R. Inaba, Sens. Actuators, B Chem. **353**, 131047 (2022)
21. G.M. Khairy, A. Duerkop, Sens. Actuators, B Chem. **281**, 878 (2019)
22. P.S. Minz, C.S. Saini, RGB camera-based image technique for color measurement of flavored milk. Measurement Food **4**, 100012 (2021)
23. Y.F. Wang, L. Li, M. Jiang, X. Yang, X. Yu, L. Xu, Appl. Surf. Sci. **573**, 151457 (2022)
24. M. Razavi, A. Barras, M. Ifires, A. Swaidan, M. Khoshkam, S. Szunerits, M. Kompany-Zareh, R. Boukherroub, J. Colloid Interface Sci. **613**, 384 (2022)
25. V. Nayak, K.R. Singh, R. Verma, M.D. Pandey, J. Singh, and R. Pratap Singh, Mater Lett **313**, 131769 (2022)
26. R. Khursheed, K. Dua, S. Vishwas, M. Gulati, N.K. Jha, G.M. Aldhafeeri, F.G. Alanazi, B.H. Goh, G. Gupta, K.R. Paudel, P.M. Hansbro, D.K. Chellappan, S.K. Singh, Biomed. Pharma. **150**, 112951 (2022)
27. H. Han, S. Li, Y. Zhong, Y. Huang, K. Wang, Q. Jin, J. Ji, K. Yao, Asian J. Pharm. Sci. **17**, 35 (2022)
28. N.A.N. Hanafy, Int. J. Biol. Macromol. **182**, 1981 (2021)
29. Q. Wen, Y. Zhang, T.A. Muluh, K. Xiong, B.Q. Wang, Y. Lu, Z.X. Wu, Y.L. Liu, H. Shi, S.S. Xiao, S.Z. Fu, Int. J. Biol. Macromol. **193**, 228 (2021)
30. Y. Nakamura, A. Mochida, P.L. Choyke, H. Kobayashi, Bioconjug. Chem. **27**, 2225 (2016)
31. B. Liu, W. Wang, J. Fan, Y. Long, F. Xiao, M. Daniyal, C. Tong, Q. Xie, Y. Jian, B. Li, X. Ma, W. Wang, Biomaterials **217**, 119301 (2019)
32. S. Yasmin-Karim, M. Moreau, W. Ngwa, In Vitro Study of Small-Sized Nanoparticle-Aided Radiation Therapy for Prostate Cancer. Intern J Radiat Oncol Biol Phy **96**, 696 (2016)
33. T. Mosmann, J. Immunol. Methods **65**, 55 (1983)

34. E. Tan, İM. Kahyaoğlu, S. Karakuş, A sensitive and smartphone colorimetric assay for the detection of hydrogen peroxide based on antibacterial and antifungal matcha extract silver nanoparticles enriched with polyphenol. Poly Bullet. **14**, 1–27 (2021)
35. B. Zheng, J. Li, Z. Zheng, C. Zhang, C. Huang, J. Hong, Y. Li, J. Wang, Opt. Laser Technol. **133**, 106522 (2021)
36. L. Engel, I. Benito-Altamirano, K.R. Tarantik, C. Pannek, M. Dold, J.D. Prades, J. Wöllenstein, Sens. Actuators, B Chem. **330**, 129281 (2021)
37. J. Chen, B. Karmakar, M.A. Salem, A.Y. Alzahrani, M.Z. Bani-Fwaz, M.M. Abdel-Daim, A.F. El-kott, Arab. J. Chem. **15**, 103681 (2022)
38. N. Halib, Z. Adam, M. Mahmud, J Appl Pharm Sci **11**, 15 (2021)
39. X. Xi, A. Pizzi, L. Delmotte, Polymers **10**, 402 (2018)
40. A.A. Oun, J.W. Rhim, Food Hydrocoll **67**, 45 (2017)
41. D. Zhu, L. Wang, W. Yu, H. Xie, Sci Rep **8**, 1 (2018)
42. K. Velsankar, S. Suganya, P. Muthumari, S. Mohandoss, S. Sudhahar, J Environ Chem Eng **9**, 106299 (2021)
43. S. Sundar, G. Venkatachalam, S.J. Kwon, Nanomaterials **8**(10), 823 (2018). https://doi.org/10.3390/nano8100823
44. I. Kumar, P. Ranjan, A.R. Quaff, J. Environ. Health Sci. Eng. **18**, 1131 (2020)
45. U. Nishan, U. Sabba, A. Rahim, M. Asad, M. Shah, A. Iqbal, J. Iqbal, N. Muhammad, Mater. Chem. Phys. **262**, 124289 (2021)
46. M. Ni, J. Chen, C. Wang, Y. Wang, L. Huang, W. Xiong, P. Zhao, Y. Xie, J. Fei, Microchem. J. **178**, 107410 (2022)
47. S.E. Elugoke, O.E. Fayemi, A.S. Adekunle, B.B. Mamba, T.T.I. Nkambule, E.E. Ebenso, FlatChem **33**, 100372 (2022)
48. V Rajeshwari C Vedhi J Fernando 2022 Dopamine sensor based on coreshell poly paraphenylene diamine/titanium dioxide/multi-walled carbon nanotube nanocomposite Mater Today: Procee
49. Y. Dong, J. Liu, J. Zheng, Colloids Surf., A **608**, 125617 (2021)
50. S. Reddy, B.E. Kumara Swamy, H. Jayadevappa, CuO nanoparticle sensor for the electrochemical determination of dopamine. Electrochim. Acta **61**, 78 (2012)
51. U. Nishan, R. Gul, N. Muhammad, M. Asad, A. Rahim, M. Shah, J. Iqbal, J. Uddin, A.-H. Ali Shah, S. Shujah, Colorimetric based sensing of dopamine using ionic liquid functionalized drug mediated silver nanostructures. Microchem. J. **159**, 105382 (2020)
52. M. Nikzamir, A. Akbarzadeh, Y. Panahi, J Drug Deliv Sci Technol **61**, 102316 (2021)
53. J.K. Fard, S. Jafari, M.A. Eghbal, Adv Pharm Bullet **5**, 447 (2015)
54. L. Chen, L.Y. Wu, W.X. Yang, Nanoparticles induce apoptosis via mediating diverse cellular pathways. Nanomedicine **13**, 2939 (2018)
55. A. P. Nikam, M. P. Ratnaparkhiand, and S. P. Chaudhari, **3**, 1121 (n.d.).
56. P. Zhao, M. Li, Y. Chen, C. He, X. Zhang, T. Fan, T. Yang, Y. Lu, R.J. Lee, X. Ma, J. Luo, G. Xiang, Int. J. Pharm. **570**, 118638 (2019)
57. J.A. Roacho-Pérez, E.N. Garza-Treviño, P. Delgado-Gonzalez, Z. G-Buentello, J.L. Delgado-Gallegos, C. Chapa-Gonzalez, M. Sánchez-Domínguez, C.N. Sánchez-Domínguez, J.F. Islas, Target Nanoparticles against Pancreatic Cancer: Fewer Side Effects in Therapy. Life **11**, 1187 (2021)
58. F.U. Din, W. Aman, I. Ullah, O.S. Qureshi, O. Mustapha, S. Shafique, A. Zeb, Int. J. Nanomed. **12**, 7291 (2017)